HHS Public Access

Author manuscript

ACS Appl Mater Interfaces. Author manuscript; available in PMC 2023 July 18.

Published in final edited form as:

ACS Appl Mater Interfaces. 2023 January 18; 15(2): 2737–2746. doi:10.1021/acsami.2c20098.

Poly(ethylene glycol)-Norbornene as a Photo-Click Bioink for Digital Light Processing 3D Bioprinting

Min Hee Kim[1,2], **Chien-Chi Lin, PhD.**[1,*]

[1]Department of Biomedical Engineering, Purdue School of Engineering & Technology, Indiana University-Purdue University Indianapolis, Indianapolis, IN 46202, USA

[2]Department of Biomedical Engineering, Texas A&M University, College Station, TX, 77843, USA

Abstract

Digital light processing (DLP) bioprinting is an emerging technology for 3D bioprinting (3DBP) owing to its high printing fidelity, fast fabrication speed, and higher printing resolution. Low viscosity bioink such as poly(ethylene glycol) diacrylate (PEGDA) is commonly used for DLP-based bioprinting. However, the crosslinking of PEGDA proceeds via chain-growth photopolymerization that displays significant heterogeneity in crosslinking density. In contrast, step-growth thiol-norbornene photopolymerization is not oxygen inhibited and produces hydrogels with an ideal network structure. The high cytocompatibility and rapid gelation of thiol-norbornene photopolymerization has lend itself to the crosslinking of cell-laden hydrogels but has not been extensively used for DLP bioprinting. In this study, we explored 8-arm PEG-norbornene (PEG8NB) as a bioink/resin for visible light initiated DLP-based 3DBP. PEG8NB-based DLP resin showed high printing fidelity and cytocompatibility even without the use of any bioactive motifs and high initial stiffness. In addition, we demonstrated the versatility of PEGNB resin by printing solid structures as cell culture devices, hollow channels for endothelialization, and microwells for generating cell spheroids. This work not only expands the selection of bioinks for DLP-based 3DBP, but also provides a platform for dynamic modification of the bioprinted constructs.

Graphical Abstract

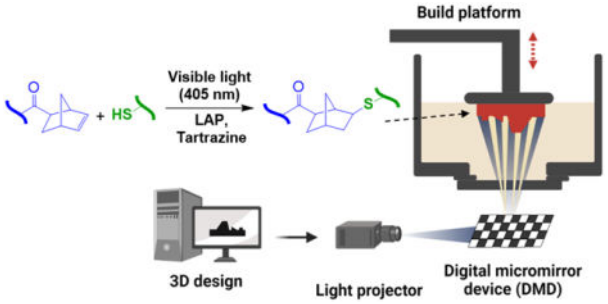

*To whom correspondence should be sent: Chien-Chi Lin, PhD. Thomas J. Linnemeier Guidant Foundation Endowed Chair & Professor, Department of Biomedical Engineering, Purdue School of Engineering & Technology, Indiana University-Purdue University Indianapolis, 723 W. Michigan St. SL220K, Indianapolis, IN 46202, USA, Phone: (317) 274-0760, lincc@iupui.edu.

Keywords

Polyethylene glycol; 3D printing; Digital light process; in vitro model; Thiol-norbornene click reaction

1. Introduction

3D bioprinting (3DBP) has emerged as a paradigm shifting technology in tissue engineering and regenerative medicine.[1–3] Commonly used 3DBP techniques include extrusion-based, nozzle-based, and vat polymerization based bioprinting. In extrusion and nozzle-based bioprinting, bioinks are extruded and layered on existing printed areas to form 3D constructs. The bioink can be loaded with cells and the printed structures are typically cured post-printing through photopolymerization. Commonly used bioinks for extrusion/nozzle-based 3DBP include derivatives of poly(ethylene glycol) (PEG)[4, 5] A variety of bio-orthogonal click chemistry reagents are now commercially available for modifying PEG and other biomacromolecules for 'clickable' crosslinking using orthogonal chemistry, including step growth thiol-ene photopolymerization, Michael type addition, inverse-electron demand Diels-Alder reaction, and SPAAC reaction.[6] Multi-arm PEG-based macromers are popular choices for chemically crosslinking into hydrogels with tunable degradability, stiffness, and permeability.[7] These click hydrogels are also increasingly being used for 3DBP applications.[5, 8–10] Despite these advantages, many multi-arm PEG-based macromers are not suitable for extrusion based bioprinting due to the low viscosity of the macromers even at a high concentration. One method to overcome the low-viscosity issue of PEG-based bioinks in extrusion-based 3DBP is to blend in rheological modifier (i.e. cellulose nanofiber, methylcellulose, nanosilicate) such that the composite bioink would exhibit desired flow behavior.[11, 12] Alternatively, a viscous bath containing gelatin microbeads, Carbopol, or nanosilicate may be used to support the printing of self-standing structure with other crosslinking mechanisms. Nonetheless, extrusion and nozzle-based bioprinting often produce various degrees of shear stress in bioink, which may cause cellular damage during the fabrication process[12–17]. In contrast to extrusion based 3DBP, vat polymerization-based 3DBP techniques such as stereolithography (SLA)[18–20], digital light process (DLP)[21–23], two-photon polymerization (2PP)[24, 25], and material jetting[2] displayed high fabrication speed and printing fidelity.[12, 26, 27] Typically, constructs are printed in a fashion by light-mediated polymerized layer of photo-responsive bioink onto a build platform.[28] This contribution focuses on DLP 3DBP as it permits layer-by-layer or volumetric projection rather than point-by-point or line-by-line printing such as the case in SLA and extrusion printing formats.[26] Added to these benefits is that the bioinks used in DLP 3DBP do not require high viscosity, permitting printing of smooth surface with fast printing time.[29]

A typical DLP printer is composed of an array of millions of micromirrors, each corresponding to a pixel in the displayed image and can be digitally modulated to design patterns to enable selective light penetration and crosslinking. Various photo-crosslinkable biomaterials with vinyl derivatives have been increasingly used for DLP 3DBP.[16, 30–32] For example, Grigoryan *et al.* described DLP printing of intravascular and multi-vascular hydrogel constructs using PEGDA and photoinitiator lithium phenyl-2,4,6-

trimethylbenzoylphosphinate (LAP) under 405 nm light.[30] Tartrazine, a yellow food dye, was used as a photoabsorber to prevent over-curing in areas outside of the desired regions during printing.[33] The DLP-printed hydrogels were used for studying functional vascular topologies. In another example, Bobrin *et al.* designed nanoscale morphological controlled multi-component DLP 3DBP. These hydrogel composed of PEGDA, acrylic acid, and poly(n-butyl acrylate)diphenyl(2,4,6-trimethylbenzoyl)phosphine oxide (TPO). The microstructure of constructs were varied by separation of block copolymer after polymerization, and the resulting materials display tunable sequence spacing and sum-10 nm domain size, and mechanical performance was found to be significantly enhanced upon the generation of microphase-separated morphologies.[34] Wang *et al.* used a microfluidic chaotic mixing chip to produce gradients of PEGDA and GelMA for DLP 3DBP.[21] However, to obtain superior printing fidelity, high concentrations of PEGDA (40%) and photoinitiator (2 mM/20 mM Ru/SPS) were used, which may reduce cell viability during printing.

Most current bioinks for DLP 3DBP are all based on chain-growth photopolymerization, with PEGDA or gelatin-methacryloyl (GelMA) as the major macromers. Compared with chain-growth PEGDA crosslinking, step-growth thiol-norbornene (NB) photopolymerization is not inhibited by dissolved oxygen, hence producing a faster crosslinking kinetics that requires a substantially lower radical concentration for initiation.[35, 36] Due to its various merit for biological applications, thiol-NB photocrosslinking has been extensively used in biomedical applications.[4, 37, 38] However, its use in DLP 3DBP has been limited. In this work, we report a norbornene functionalized 8-arm PEG (PEGNB) as a resin for DLP 3DBP. We systematically characterized the rheological properties and printability of the PEGNB resin system consisting of PEGNB, tartrazine, and LAP. Furthermore, we rendered the otherwise inert PEGNB hydrogel network bioactive through facile secondary conjugation of integrin-binding motif (CRGDS). Finally, we demonstrated the usefulness of PEGNB as a DLP resin by printing various 3D structures that support *in vitro* cell culture.

2. Experimental

2.1. Materials

8-arm PEG (20 kDa) was obtained from JenKem Technology USA. 4-arm-PEG-SH (PEG4SH,10 kDa) was purchased from Laysan Bio. Lithium phenyl-2,4,6 trimethylbenzoyl-phosphinate (LAP), tartrazine, and *N,N'*-dicyclohexyl-carbodiimide (DCC) were purchased from Sigma-Aldrich. Dichloromethane (DCM) and pyridine were purchased form Acros Organics Chemicals. 4-(dimethylamino)pyridine (DMAP) was purchased from Alfa Aesar. Diethylether was purchased from VWR. All reagents were used as received without further purification.

2.2. PEG8NB synthesis

8-arm PEG-norbornene (PEG8NB) was synthesized according to our established protocol with slight modification.[38] Briefly, DCC was reacted with norbornene acid in DCM to form an intermediate product - norbornene carboxylic acid O-acyl-urea, followed by the formation of norbornene anhydride and by-product dicyclohexylurea. Norbornene anhydride was filtered into a second flask containing pre-dissolved 8-arm PEG-OH, DMAP, and

pyridine in DCM. The flask was purged with nitrogen and placed in an ice bath. The reaction was allowed to proceed overnight, and the product was filtered and then precipitated in cold diethyl ether. The precipitated product was re-dissolved in D.I. water and purified by dialysis (Spectra, MWCO: 3,500) against D.I. water for 7 days and lyophilized until dried. Proton nuclear magnetic resonance (1H NMR, 500 MHz, ADVANCE III, Bruker) was used to confirm the conversion of PEG8NB with respect to the norbornene group (Fig. S1).

2.3. Hydrogel fabrication

PEG8NB hydrogels were crosslinked by mixing PEG8NB (final conc. 3–9 wt%) with PEG4SH at a stoichiometric ratio of thiol to norbornene groups. Photoinitiator LAP (final conc. 2–15 mM) and photoabsorber tartrazine (final conc. 0–2 mM) were added and i*n situ* photo-gelation studies were conducted using an oscillatory rheometer (MCR 102, Anton Paar). Briefly, precursor solution was placed on the lower plate and the flat geometry (25 mm plate) was lowered to 100 μm and *in situ* rheometry was performed in time sweep mode (5% strain at 1 Hz) at 25°C. Visible light (OmniCure Series 2000, 400–500 nm filter) was turned on 10 s after starting the measurement. Disc shape (8 mm diameter and 1 mm thickness) PEG8NB hydrogels were DLP-printed for measuring shear moduli. The DLP-printed gel discs were carefully transferred to the rheometer prior to initiating the measurements and the frequency sweep test was conducted at 1% strain.

2.4. DLP 3D printing of PEG8NB

PEG8NB was dissolved in PBS to a final concentration of 3 to 9 wt% along with PEG4SH (thiol to NB ratio=0.8), LAP (10 mM), and tartrazine (1.5 mM) to form PEG8NB hydrogel. A DLP printer (LumenX+, Cellink) was used to produce all 3DBP samples. A 405 nm LED light was used to project patterns of precise light exposure (10.3–19.2 mW/cm^2, 5–20 s) onto the PEG8NB printing resin. Printing shapes were generated from TinkerCad website and converted to STL file using Cellink Heartware software. Designed STL files were then input into DLP printer and constructs were printed onto a PDMS-coated petri dish. After printing was completed, the DLP printed hydrogels were removed from the build platform and washed with PBS to remove unreacted resin. DLP printed PEG8NB hydrogels were immersed in fluorescein solution for 30 min (2 mg/ml in ethanol), then transferred to glass slides for imaging with Lionheart fluorescence microscope (BioTek).

2.5. Post-printing surface modification

Pancreatic cancer cells (COLO-357), NIH 3T3 fibroblasts, and mouse mesenchymal stem cells (mMSCs) were cultured using DMEM high glucose (Gibco™) supplemented with 10% fetal bovine serum (FBS, Corning), and 1% pentamycin/streptomycin (P/S, Life Technologies). Human umbilical vein endothelial cells (HUVECs) were cultured using endothelial cell medium (ECM, ScienCell Research Laboratories, Inc.) supplemented with 2% FBS, endothelial cell growth supplements, and antibiotic solution.

A secondary thiol-norbornene photoclick reaction was performed on the surface of DLP-printed PEG8NB hydrogels to render the surface adhesive to cells. Briefly, a solution containing 5 mM CRGDS peptide and 2 mM LAP was added in the DLP-printed PEG8NB multi-well devices or hollow channels hydrogels, followed by exposing the devices to 365

nm light at 5mW/cm^2 for 2 minutes. The modified devices were rinsed with PBS to remove unreacted species. The post-gelation surface modification was also performed with thiolated rhodamine for imaging purpose.

2.6. Cell culture in DLP-printed devices

For 2D cell culture, 1×10^5 of NIH 3T3 fibroblasts were seeded on the DLP-printed hydrogels with or without secondary RGD conjugation. After 24 h, hydrogels were fixed with 4% paraformaldehyde and blocked with 1% bovine serum albumin (BSA) at 4°C overnight. Samples were then stained with rhodamine phalloidin (1:200) and DAPI (1:1000) to visualize F-actin and nuclei, respectively. In case of direct 3D encapsulation, mMSCs cells were mixed with sterile-filtered (0.22 μm) PEG8NB resin (5 wt%), LAP (10 mM), and tartrazine (1.5 mM) and disc-shaped cell-laden hydrogels were printed. Post-printing, the cell-laden hydrogels were placed in a non-treated 24-well plate. Cell culture media were refreshed every 2 days. At predetermined time period (Day 2, 4, and 7), cell-laden hydrogels were stained with Live/Dead staining kit.

For endothelialization of the DLP-printed microchannels, HUVECs (density: 1×10^6 cells/ml) were seeded within the microchannels and cultured for 2 to 4 days. The endothelialized samples were fixed with 4% paraformaldehyde and block with 1% BSA at 4°C overnight. The cells were then stained with VE-cadeherin (1:2), rhodamine phalloidin (1:200), and DAPI (1:1000) for visualizing the formation of endothelial cell monolayer. For cancer cell spheroid formation, COLO-357 cells were seeded into the DLP printed 3D microwells at a density of 2,000–10,000 cell per microwells, which were placed in a 24-well plate. The plate was centrifuged at 500 rpm for 5 min to facilitate cell aggregate formation. Extra cells outside of the microwells were removed with a gentle flow of media and cultured for 48 h to form cancer cell spheroids. Cell spheroid viability was determined using ReadyProbes™ Cell Viability Imaging Kit (Blue/Green) according to manufacturer's protocol. Furthermore, samples were stained with rhodamine phalloidin (1:200) and DAPI (1:1000) to visualize F-actin and nuclei, respectively. Samples were imaged by a laser scanning confocal microscope (Olympus Fluoview FV100). All image processing and analyses were conducted by ImageJ. Thereafter, cell area and circularity were determined based on manual thresholding of isolated cells[31].

2.7. Statistical analysis

All statistical analyses were performed using GraphPad Prism 8 software. Significance comparison between experimental groups were performed using two-tailed t-test, for two-group comparison, and two-way ANOVA with Bonferroni's post testing. All experiments were conducted a minimum of three times with data presentation as the mean ± standard error of the mean (SEM). *, **, *** represent $p < 0.05$, 0.01, or 0.001, respectively.

3. Results and Discussion

3.1. Optimization of visible light-initiated thiol-norbornene photocrosslinking for DLP printing

Through step-growth photopolymerization, PEG8NB orthogonally crosslinked with PEG4SH into a hydrogel network with thiol-ether linkages (Fig. 1a). To ensure the visible light source (405 nm) installed on the LUMEN X+ DLP printer could emit light intensity suitable for thiol-norbornene crosslinking, we first measured the light intensity within the middle range of light power output (25% to 40%). As shown in Fig. S2, light intensities were measured at 10.3, 13.4, 16.2, and 19.2 mW/cm^2 for 25%, 30%, 35%, and 40% power output, respectively. This range of light intensities were commonly used for in situ cell encapsulation. Using *in situ* visible light photo-rheometry at 25% light power output setting, we evaluated thiol-NB hydrogel crosslinking kinetics. A typical formulation of 5 wt% PEG8NB (20 kDa), 4 wt% PEGSH (10 kDa) ($R_{thiol/NB}$=0.8), and 10 mM photoinitiator LAP led to G'/G" crossover (gel point) in less than 1 second and complete gelation in 3 seconds upon light irradiation (0 mM tartrazine. Fig. 1b). The addition of tartrazine, a photoabsorber commonly used in DLP to reduce off-focal-plane polymerization,[22, 30] delayed the gel point but only by a few seconds (6 seconds for 1.5 mM tartrazine added. Fig. 1b). Of note, as tartrazine competed with LAP for the lmited photons emitted from the light source, at a concentration over 2 mM it completely prevented thiol-NB gelation (data not shown). While the addition of tartrazine from 0.5 to 1.5 mM delayed gel points, it did not alter the plateau moduli (G' ~20 kPa) of the crosslinking. At a constant tartrazine concentration (i.e., 1.5 mM), increasing photoinitiator LAP concentration led to faster G'/G" crossover (Fig. 1c), with the gel point decreased from 12 seconds to 3 seconds when LAP concentration was increased from 2 mM to 15 mM. Altering LAP concentration from 5 to 15 mM decreased the time to reach gel point (8 to 3 seconds), but all formulations reached similar plateau moduli (G' ~ 20 kPa) in less than 15 seconds. Next, tartrazine and LAP concentrations were fixed at 1.5 and 10 mM, respectively, while altering PEG8NB and thiol/NB molar ratio (i.e., [SH]/[NB]), two parameters directly impacting the contents reactive groups. As the PEG8NB concentration was increased from 3 wt% to 9 wt%, the gel point varied slightly between 3 to 6 seconds but the plateau moduli increased significantly from ~7 kPa to ~43 kPa (Fig. 1d). Similarly, decreasing [SH]/[NB] from 1 to 0.2 drastically delayed gel point from 3 to 15 seconds and reduced plateau moduli from ~22 kPa to ~ 0.2 kPa (Fig. 1e).

It is worth noting that the wavelenghts of light used to initiate thiol-norbornene photopolymerization depends on the chosen photoinitiator. For example, thiol-NB photopolymerization can be initiated by type 1 (cleavage-type) photoinitiator lithium phenyl-2,4,6-trimethylbenzoylphosphinate (LAP), which is photolysed to generate radical species by lights with wavelengths from 280 nm to 405 nm.[39–41] Alternatively, thiol-NB photopolymerization can also be initiated by type 2 photoinitiator (or sensitizer), such as eosin-Y at visible light wavelengths (400–700 nm).[42, 43] Once the radical species are generated from exicted photoinitiators, they quickly extract protons from nearby sulfhydryl moieties, forming thiyl radicals that then propagate through the unsaturated ring-strained norbornene bonds on PEG8NB.[35, 44] This reaction produces a carbon-center radical on NB that attacks another thiol group to form a covalent thiol-ether bond and regenerate the thiyl

radical for the next thiol-norbornene click reaction. The photoclick reactions continue until one of the functional groups (thiol or NB) is completely consumed. For UV light (e.g., 365 nm) induced thiol-NB reaction, a LAP concentration of less than 2 mM would be sufficient to initiate hydrogel crosslinking, with a G'/G" crossover typically occurred within 10 seconds due to the high light sensitivity of LAP at UV light wavelengths.[45–48] While the absorbance of LAP peaks at 370 nm, it tailed off rapidly with only 14.1% of absorbability remained at 405 nm.[49] Increasing LAP concentration to 10 mM addressed this issue and markedly accelerated gelation kinetics under visible light irradiation. These optimization works established the basic parameters critical in 3D printing of PEG8NB using a DLP printer. Importantly, our optimized thiol-NB crosslinking conditions compared favorably to that using diacrylate-based DLP resin. In one example, 20% PEGDA and 34 mM LAP were used for DLP 3D printing.[50]

3.2. Printability of PEGNB using a DLP printer

In DLP printing, 3D models are first stacked into horizontal layers in the form of black and white image files, forming a 'mask' where light can only penetrate through the white space. A visible-light projector (405 nm), which is controlled by digital micromirror (DMD), then emits light through the 'mask' and projects on a droplet of liquid bioink/resin kept in a polydimethylsiloxane (PDMS) chamber (Fig. 2a). The sol-gel transition of the bioink occurs only in the region exposed to light in as little as a few seconds depending on the bioink formulations. The light-based curing proceeds in a layer-by-layer fashion (50–100 μm per layer) until the whole construct is printed. To test the DLP printing fidelity using PEG8NB/PEG4SH as the resin, we designed various simple geometrical shapes (e.g., triangle, square, hexagon, and circle. Fig. 2b). The resin was composed of 5 wt% PEG8NB, 4 wt% PEG4SH ($R_{thiol/NB}$ = 0.8), 10 mM LAP, and 1.5 mM tartrazine. After printing, the constructs (5 mm thickness) were imaged and characterized for their printing fidelity. During the printing, the first 2 layers were exposed with light for 30 s to improve adhesion with the build platform. Subsequently, additional 48 layers were stacked with 10 s irradiation of 405 nm light, and total 50 layers of constructs were stacked (i.e., 540 seconds total print time). All DLP printed PEG8NB hydrogels demonstrated excellent structural stability (Fig. 2b) and high fidelity. The printability of PEG8NB resin was evaluated by comparing the pore area of designed and printed structure (Fig. 2c). The stiffness increased from 2.7 kPa to 20 kPa with increasing PEG8NB concentration (3 wt% to 9 wt%) and the printed constructs did not undergo significant degradation/swelling over 7 days in PBS (Fig. 2d). The capability of the PEG8NB resin to form complex scaffolds with high fidelity despite the low macromer/photoinitiator concentration is notable and structures as tall as 5 mm height can be 3D printed in 9 min without the need for any support. The current results were derived using a commercial DLP printer with a minimum pixel resolution of 50 μm.

3.3. DLP-printed cell culture models

We next explored the use of DLP printed PEG8NB hydrogels as cell culture devices. For materials intended to interface with cells, it is imperative for the surface of the materials to provide desired cell binding motifs. Like PEGDA, PEG8NB does not provide any cell-adhesive ligands owing to the 'stealth' properties of PEG. Different from PEGDA, however, PEG8NB can be modified post-gelation through a secondary orthogonal thiol-norbornene

click reaction, given that excess unreacted NB groups are available post printing (Fig. 3a).[51, 52] To this end, we printed a PEG8NB-based well device for 2D cell culture (Fig. 3b). After printing, 5mM CRGDS and 2mM photoinitiator LAP were added in three of the six wells and secondary surface immobilization was performed under 1 min of light exposure (365 nm, 5 mW/cm^2). The same thiol-NB reaction that crosslinked the hydrogels now served as a means to immobilized integrin ligand CRGDS (Fig. 3a). After washing off unconjugated CRGDS, NIH 3T3 fibroblasts were seeded/cultured on the surface and stained for F-actin for visualization of the cell spreading. After 24 h of incubation, cells attached extensively on the surface of the wells with CRGDS immobilization, while no spindle shaped cells were observed in the wells without CRGDS conjugation (Fig. 3c). Through image analysis, we confirmed higher number (Fig. 3d) and lower circularity (Fig. 3e) of the adhered cells, indicating that the surface of the CRGDS-immobilized DLP-printed PEG8NB wells supported cell attachment. While not characterized in this study, increased cell adhesion may lead to integrin activation, resulting in the formation of focal adhesions.[53] It is possible to immobilize multiple peptide ligands (i.e. fibronectin, laminin, vitronectin-derived peptides) to synergistically enhance integrin activation. While not demonstrating in this contribution, the biological properties of DLP printed PEG8NB hydrogel may be also tuned using other click chemistry such as tetrazine-NB inverse electron-demand Diels-Alder Reaction (iEDDA).[46, 48, 54]

In addition to culturing cells on the surface of the DLP-printed PEG8NB hydrogels, we also attempted to encapsulate cells during DLP printing. We found that cells encapsulated in the DLP-printed hydrogels remained mostly alive, with a viability of over 70%. (Fig. S3). We culture the cell-laden DLP-printed PEG8NB hydrogels and found that cell viability decreased considerably during long-term culture (> 7 days). The relatively low cell viability could be attributed to the relatively high crosslinking density and stiffness of the DLP-printed hydrogels. High crosslinking density is generally desired for high printing fidelity but at the expense of tissue-mimetic matrix stiffness and cell viability. In this regard, Wang et al. developed a selective enzymatic degradation approach to modulate the stiffness of DLP-printed hyaluronic acid-gelatin hybrid hydrogels for matching mechanical properties of various tissues[55]. While enzyme-mediated degradation high molecular weight of HA led to higher degree of cell spreading and function, no cell proliferation was observed in the HA/gelatin hybrid hydrogel due to the stiffness. While in this work, we achieved a reasonably high initial cell viability (>70%) in the DLP-printed hydrogels, the current hydrogels did not contain any bioactive motifs, such as cell binding ligand or MMP degradable sequence. It is likely that the encapsulated cells may be more viable for a longer time if the PEG8NB hydrogel was printed in the presence of cell adhesive ligands or protease-labile linkers[56, 57]. It is also possible that conducting DLP printing using PEG8NB macromers with higher hydrolytic degradability may result in hydrogels with more tunable moduli and favorable cell viability within the printed hydrogels[45, 58] However, such endeavors require a renewed optimization of DLP printing parameters. In the subsequent studies, we would focus on the use of DLP-printed 3D structures for different potential biomedical applications.

3.4. Perfusable channel printing

One major benefit of 3DBP is to create complex tunnel structures to enable perfusion cell culture.[50, 59] To this end, we employed DLP printing to fabricate PEG8NB hydrogels with tunnel structures that can be used for forming microvasculature. A serpentine tunnel with 1 mm diameter was selected to evaluate the printing fidelity (Fig 4). First, we conducted DLP 3D printing of a serpentine tunnel using different 5 wt% PEG8NB, R=0.8 with PEG4SH, 10 mM LAP, and 1.5 mM tartrazine. We tested the printing fidelity using different light level/intensity and exposure time (Fig 4a). No perfusable channel was obtained at a lower light intensity setting (25%, 10.3 mW/cm^2) regardless of curing time (5 to 20 s per layer), although this light intensity was sufficient in printing solid structures (Figs. 1–3). Increasing light intensity setting to 30% while keeping the curing time to under 10 seconds per layer led to channels that were perfusable (Fig. 4b, 4c) with a designed diameter (1 mm, Fig. S4). At 30% light intensity setting, extending the curing time to 15 seconds per layer resulted in perfusble but narrowing channel diameter (~0.8 mm, Fig. S4). Further increasing the curing time to 20 seconds per layer led to non-perfusable channel (Fig. 4a, 4b) due to over-curing of the PEG8NB hydrogels. This phenomenon was similar to that with a lower photoabsorber concentration (e.g., 1 mM, Fig. S5), where the printed structure was over-cured due to the efficient thiol-NB photocrosslinking. At a light setting of 35% to 40%, perfusable channels with the designed channel diameter were obtained only when curing time per layer was kept at below 10 to 5 seconds, respectively (Fig. 4a, 4b). Note that at 35% light intensity and 15 seconds per layer curing time, some prints resulted in narrow and perfusable channels but others were printed with occluded channels. These optimization results highlighted the importance to adjust printing parameters for creating hollow structures.

As described in Fig. 3, thiol-norbornene photopolymerized PEG8NB hydrogels permit secondary modification post-gelation. We further tested this feature in the perfusable channel by immobilizing thiolated Rhodamine (Rho-SH). We injected 1 mM LAP and Rho-SH solution into the channel, followed by exposing the hydrogel under 365 nm light for 1 min. The secondary Rho-SH immobilization was confirmed by fluorescence microscopy as shown in Fig. 4d. In addition to the single serpentine tunnel structure, DLP printing of independent multichannel structure using PEG8NB was also successful (Fig. 4e), as shown by the separation of the two-color dye solutions (green and red) injected into the two channels.

Next, we sought to create an *in vitro* vascular model using the DLP printed channels. A channel diameter of 600 μm was selected for facile formation of a vessel recapitulating the size of an artery[60]. Arrays of straight channels were printed on a supporting layer (Fig. 5a), which was removed after printing (Fig. 5b). After DLP printing, the surface of the channels was conjugated with cell adhesive CRGDS peptide as described in Fig. 4d. Next, human umbilical vein endothelial cells (HUVECs, 10 M cells/ml) were seeded inside of the channel and cultured for 4 days. Before immersing the hydrogel into the media, gels were inverted 180 degrees to facilitate endothelial channel formation. We found that HUVECs adhered to the surface of the entire microchannels within 2 days and formed a mono layer of cells (Fig. 5c). Furthermore, vascular endothelial-cadherin (VE-cadherin), a major adhesive protein of inter-endothelial tight junctions,[61] was detected across the channel surface and was more

localized on day 4 (Fig 5c). These results demonstrated the successful use of PEG8NB as a resin for DLP printing both solid and hollow structures. Current methods to create microvasculature in biomaterials include forming a hydrogel embedded with a removable wire (i.e. silicone, metal wire, needle) or sacrificial material (polycarbonate, poly(methyl methacrylate).[62–64] The removal of wire/tubing/needle may damage the structure of the scaffold, whereas some sacrificial materials may not be completely removed/dissolved and the resides may negatively affect cell physiology. With DLP printing, it is possible to implement a complex microvascular structure. Future work will focus on implementing a perfusion culture system on the DLP-printed microvasculature.[50]

3.5. Microwell Design for Cancer Cell Spheroid Model

Next, we designed and printed PEG8NB microwell for preparing uniform cell spheroids. The creation of PEG-based microwells used to be a laborious process involving the use of a mask aligner and photolithography.[65] DLP printing provides an alternative method to create microwells for cell culture and rapid generation of spheroids. Here, we use DLP printing to fabricate microwells that fit in wells of a 24-well plate (Fig. 6a). A cone-shape design was selected to facilitate the aggregation of the cells into spheroids (Fig. 6b). We designed microwells with three diameters, 400, 800, and 1000 μm (Fig. 6c) and seeded RFP-transduced pancreatic cancer cells COLO-357 into the DLP-printed microwells fitted in a 24-well plate. Cell clusters formed soon after seeding and plate centrifugation (Day 0, Fig. 6c), and compact spheroids were uniformly formed between 24 h to 48 h and remained relatively stable over 7 days (Fig. 6c). The sizes of the spheroids scaled with, but were consistently smaller than, the microwell diameter (Fig. 6c, 6d). Through live/dead staining, we showed that a few dead cells were observed in the center of the spheroids and cells near the periphery area of the spheroids were mostly alive (Fig. 6e), suggesting the cytocompatibility of the DLP-printed microwells. Finally, we designed microwells with different geometry (e.g., triangle, square, and star) to generate spheroids with different shapes (Fig. 6f). PEG-based microwells are increasingly used for generating spheroids. For example, Lutolf and colleagues built an organoid array technology using PEG-based microwells,[66] which were generated using silicon-based soft lithography and PDMS molding. The PDMS molds were then used to imprint thiol-vinylsulfone hydrogel crosslinking (gelatin time ~15 min). The uniform PEG-based microwells were used to reduce heterogeneity of the spheroids generated and for large-scale screening. However, this process involved several time-consuming steps and multiple instruments. In contrast, our thiol-norbornene based microwells were rapidly produced in a single step from using a DLP bioprinter and without the use of any molding materials (e.g., PDMS). The DLP printed PEG8NB microwells were also amenable for post-gelation modification, which may be useful for screening cell-materials interactions. We believe that our simple lab-scale customization using DLP 3DBP offers a promising technique for studying cell-materials interactions and for generating functional spheroids in regenerative medicine applications.

4. Conclusion

In this study, we have established PEG8NB as a new DLP printing resin. As a low viscosity bioink/resin, PEG8NB solution was printed into hydrogels with high printing fidelity by

the efficient orthogonal thiol-norbornene photo-click reaction, which was amenable for post-printing modification of hydrogel surface. We demonstrated this by post-printing conjugation of RGDS peptide on flat surfaces and in microchannels. DLP-printed PEG8NB hydrogels showed excellent printability even at low photoinitiator and photoabsorber concentrations, and were applicable to various *in vitro* cell culture models, including formation of endothelialized channels and multi-cell spheroids. This study has demonstrated the potential of PEG8NB as a novel photo-responsive resin for DLP bioprinting applications.

Supplementary Material

Refer to Web version on PubMed Central for supplementary material.

Acknowledgement

This project was supported in part by the National Cancer Institute (R01CA227737, to CL), National Institute of Diabetes and Digestive and Kidney Diseases (R01DK127436, to CL) and the Basic Science Research Program through the National Research Foundation of Korea (NRF) funded by the Ministry of Education (2021R1A6A3-A14044259, to MHK).

Reference

1. Wang Q; Sun J; Yao Q; Ji C; Liu J; Zhu Q, 3D Printing with Cellulose Materials. Cellulose 2018, 25 (8), 4275–4301.
2. Ng WL; Chua CK; Shen Y-F, Print Me An Organ! Why We Are Not There Yet. Prog. Polym. Sci 2019, 97, 101145.
3. Matai I; Kaur G; Seyedsalehi A; McClinton A; Laurencin CT, Progress in 3D Bioprinting Technology for Tissue/Organ Regenerative Engineering. Biomaterials 2020, 226, 119536. [PubMed: 31648135]
4. Lin C-C; Anseth KS, PEG Hydrogels for the Controlled Release of Biomolecules in Regenerative Medicine. Pharm. Res 2009, 26 (3), 631–643. [PubMed: 19089601]
5. Xin S; Chimene D; Garza JE; Gaharwar AK; Alge DL, Clickable PEG Hydrogel Microspheres as Building Blocks for 3D Bioprinting. Biomater. Sci 2019, 7 (3), 1179–1187. [PubMed: 30656307]
6. Arkenberg MR; Nguyen HD; Lin C-C, Recent Advances in Bio-Orthogonal and Dynamic Crosslinking of Biomimetic Hydrogels. J. Mater. Chem. B 2020, 8 (35), 7835–7855. [PubMed: 32692329]
7. Tan H; DeFail AJ; Rubin JP; Chu CR; Marra KG, Novel Multiarm PEG-based Hydrogels for Tissue Engineering. J. Biomed. Mater. Res. A 2010, 92 (3), 979–987. [PubMed: 19291691]
8. Mueller E; Poulin I; Bodnaryk WJ; Hoare T, Click Chemistry Hydrogels for Extrusion Bioprinting: Progress, Challenges, and Opportunities. Biomacromolecules 2022, 23 (3), 619–640. [PubMed: 34989569]
9. Kim MH; Lin C-C, Norbornene-Functionalized Methylcellulose as a Thermo-and Photo-Responsive Bioink. Biofabrication 2021, 13 (4), 045023.
10. GhavamiNejad A; Ashammakhi N; Wu XY; Khademhosseini A, Crosslinking Ttrategies for 3D Bioprinting of Polymeric Hydrogels. Small 2020, 16 (35), 2002931.
11. Ahlfeld T; Guduric V; Duin S; Akkineni A; Schütz K; Kilian D; Emmermacher J; Cubo-Mateo N; Dani S; Witzleben M.v.; Spangenberg J; Abdelgaber R; Richter RF; Lode A; Gelinsky M Methylcellulose–A Versatile Printing Material That Enables Biofabrication of Tissue Equivalents with High Shape Fidelity. Biomater. Sci 2020, 8 (8), 2102–2110. [PubMed: 32236265]
12. Rajput S; Deo KA; Mathur T; Lokhande G; Singh KA; Sun Y; Alge DL; Jain A; Sarkar TR; Gaharwar AK, 2D Nanosilicate for Additive Manufacturing: Rheological Modifier, Sacrificial Ink and Support Bath. Bioprinting 2022, 25, e00187.

13. Placone JK; Engler AJ, Recent Advances in Extrusion-Based 3D Printing for Biomedical Applications. Adv. Healthc. Mater 2018, 7 (8), 1701161.
14. Hidaka M; Kojima M; Nakahata M; Sakai S, Visible Light-Curable Chitosan Ink for Extrusion-Based and Vat Polymerization-Based 3D Bioprintings. Polymers 2021, 13 (9), 1382. [PubMed: 33922859]
15. Provaggi E; Kalaskar DM, 3D Printing Families: Laser, Powder, Nozzle Based Techniques. In 3D Printing in Medicine, Elsevier: 2017; pp 21–42.
16. Li W; Mille LS; Robledo JA; Uribe T; Huerta V; Zhang YS, Recent Advances in Formulating and Processing Biomaterial Inks for Vat Polymerization-Based 3D Printing. Adv. Healthc. Mater 2020, 9 (15), 2000156.
17. McCormack A; Highley CB; Leslie NR; Melchels FP, 3D Printing in Suspension Baths: Keeping the Promises of Bioprinting Afloat. Trends Biotech. 2020, 38 (6), 584–593.
18. Grigoryan B; Sazer DW; Avila A; Albritton JL; Padhye A; Ta AH; Greenfield PT; Gibbons DL; Miller JS, Development, Characterization, and Applications of Multi-Material Stereolithography Bioprinting. Sci. Rep 2021, 11 (1), 1–13. [PubMed: 33414495]
19. Miri AK; Nieto D; Iglesias L; Goodarzi Hosseinabadi H; Maharjan S; Ruiz-Esparza GU; Khoshakhlagh P; Manbachi A; Dokmeci MR; Chen S, Microfluidics-Enabled Multimaterial Maskless Stereolithographic Bioprinting. Adv. Mater 2018, 30 (27), 1800242.
20. Wang Z; Kumar H; Tian Z; Jin X; Holzman JF; Menard F; Kim K, Visible Light Photoinitiation of Cell-Adhesive Gelatin Methacryloyl Hydrogels for Stereolithography 3D Bioprinting. ACS Appl. Mater Interfaces 2018, 10 (32), 26859–26869. [PubMed: 30024722]
21. Wang M; Li W; Mille LS; Ching T; Luo Z; Tang G; Garciamendez CE; Lesha A; Hashimoto M; Zhang YS, Digital Light Processing Based Bioprinting with Composable Gradients. Adv. Mater 2022, 34 (1), 2107038.
22. Huh J; Moon Y-W; Park J; Atala A; Yoo JJ; Lee SJ, Combinations of Photoinitiator and UV Absorber for Cell-based Digital Light Processing (DLP) Bioprinting. Biofabrication 2021, 13 (3), 034103.
23. Yu C; Miller KL; Schimelman J; Wang P; Zhu W; Ma X; Tang M; You S; Lakshmipathy D; He F, A Sequential 3D Bioprinting and Orthogonal Bioconjugation Approach for Precision Tissue Engineering. Biomaterials 2020, 258, 120294. [PubMed: 32805500]
24. Liu H; Chansoria P; Delrot P; Angelidakis E; Rizzo R; Rütsche D; Applegate LA; Loterie D; Zenobi-Wong M, Filamented Light (FLight) Biofabrication of Highly Aligned Tissue-engineered Constructs. Adv. Mater 2022, 34 (45), 2204301.
25. Kelly BE; Bhattacharya I; Heidari H; Shusteff M; Spadaccini CM; Taylor HK, Volumetric Additive Manufacturing via Tomographic Reconstruction. Science 2019, 363 (6431), 1075–1079. [PubMed: 30705152]
26. Yu C; Schimelman J; Wang P; Miller KL; Ma X; You S; Guan J; Sun B; Zhu W; Chen S, Photopolymerizable Biomaterials and Light-based 3D Printing Strategies for Biomedical Applications. Chem. Rev 2020, 120 (19), 10695–10743. [PubMed: 32323975]
27. Rivera-Tarazona LK; Shukla T; Singh KA; Gaharwar AK; Campbell ZT; Ware TH, 4D Printing of Engineered Living Materials. Adv. Funct. Mater 2022, 32 (4), 2106843.
28. Sampson KL; Deore B; Go A; Nayak MA; Orth A; Gallerneault M; Malenfant PR; Paquet C, Multimaterial Vat Polymerization Additive Manufacturing. ACS Appl. Polym. Mater 2021, 3 (9), 4304–4324.
29. Choi JW; Kim G-J; Hong S; An JH; Kim B-J; Ha CW, Sequential Process Optimization for a Digital Light Processing System to Minimize Trial and Error. Sci. Rep 2022, 12 (1), 1–15. [PubMed: 34992227]
30. Grigoryan B; Paulsen SJ; Corbett DC; Sazer DW; Fortin CL; Zaita AJ; Greenfield PT; Calafat NJ; Gounley JP; Ta AH, Multivascular Networks and Functional Intravascular Topologies within Biocompatible Hydrogels. Science 2019, 364 (6439), 458–464. [PubMed: 31048486]
31. Dhand AP; Davidson MD; Galarraga JH; Qazi TH; Locke RC; Mauck RL; Burdick JA, Simultaneous One-pot Interpenetrating Network Formation to Expand 3D Processing Capabilities. Adv. Mater 2022, 2202261.

32. Ma X; Qu X; Zhu W; Li Y-S; Yuan S; Zhang H; Liu J; Wang P; Lai CSE; Zanella F, Deterministically Patterned Biomimetic Human iPSC-derived Hepatic Model via Rapid 3D Bioprinting. Proc. Natl. Acad. Sci. U.S.A 2016, 113 (8), 2206–2211. [PubMed: 26858399]
33. Yang Y; Zhou Y; Lin X; Yang Q; Yang G, Printability of External and Internal Structures based on Digital Light Processing 3D Printing Technique. Pharmaceutics 2020, 12 (3), 207. [PubMed: 32121141]
34. Bobrin VA; Lee K; Zhang J; Corrigan N; Boyer C, Nanostructure Control in 3D Printed Materials. Adv. Mater 2022, 34 (4), 2107643.
35. Fairbanks BD; Schwartz MP; Halevi AE; Nuttelman CR; Bowman CN; Anseth KS, A Versatile Synthetic Extracellular Matrix Mimic via Thiol-Norbornene Photopolymerization. Adv. Mater 2009, 21 (48), 5005–5010. [PubMed: 25377720]
36. Shih H; Lin C-C, Cross-linking and Degradation of Step-Growth Hydrogels Formed by Thiol–Ene Photoclick Chemistry. Biomacromolecules 2012, 13 (7), 2003–2012. [PubMed: 22708824]
37. Kim MH; Nguyen H; Chang C-Y; Lin C-C, Dual Functionalization of Gelatin for Orthogonal and Dynamic Hydrogel Cross-Linking. ACS Biomater. Sci. Eng 2021, 7(9), 4196–4208.
38. Lin C-C; Raza A; Shih H, PEG Hydrogels Formed by Thiol-Ene Photo-Click Chemistry and Their Effect on the Formation and Recovery of Insulin-Secreting Cell Spheroids. Biomaterials 2011, 32 (36), 9685–9695. [PubMed: 21924490]
39. Fairbanks BD; Schwartz MP; Bowman CN; Anseth KS, Photoinitiated Polymerization of PEG-Diacrylate with Lithium Phenyl-2, 4, 6-trimethylbenzoylphosphinate: Polymerization Rate and Cytocompatibility. Biomaterials 2009, 30 (35), 6702–6707. [PubMed: 19783300]
40. Greene T; Lin TY; Andrisani OM; Lin CC, Comparative Study of Visible Light Polymerized Gelatin Hydrogels for 3D Culture of Hepatic Progenitor Cells. J. Appl. Polym. Sci 2017, 134 (11).
41. Shih H; Fraser AK; Lin C-C, Interfacial Thiol-Ene Photoclick Reactions for Forming Multilayer Hydrogels. ACS Appl.Mater. Interfaces 2013, 5 (5), 1673–1680. [PubMed: 23384151]
42. Shih H; Liu H-Y; Lin C-C, Improving Gelation Efficiency and Cytocompatibility of Visible Light Polymerized Thiol-Norbornene Hydrogels via Addition of Soluble Tyrosine. Biomater. Sci 2017, 5 (3), 589–599. [PubMed: 28174779]
43. Shih H; Lin CC, Visible-Light-Mediated Thiol-Ene Hydrogelation Using Eosin-Y as the Only Photoinitiator. Macromol. Rapid commun 2013, 34 (3), 269–273. [PubMed: 23386583]
44. Lin CC; Ki CS; Shih H, Thiol–Norbornene Photoclick Hydrogels for Tissue Engineering Applications. J. Appl. Polym. Sci 2015, 132 (8).
45. Lin F-Y; Lin C-C, Facile Synthesis of Rapidly Degrading PEG-Based Thiol-Norbornene Hydrogels. ACS Macro Lett. 2021, 10 (3), 341–345. [PubMed: 35549061]
46. Arkenberg MR; Dimmitt NH; Johnson HC; Koehler KR; Lin CC, Dynamic Click Hydrogels for Xeno-Free Culture of Induced Pluripotent Stem Cells. Adv. Biosyst 2020, 4 (11), 2000129.
47. Liu H-Y; Korc M; Lin C-C, Biomimetic and Enzyme-Responsive Dynamic Hydrogels for Studying Cell-Matrix Interactions in Pancreatic Ductal Adenocarcinoma. Biomaterials 2018, 160, 24–36. [PubMed: 29353105]
48. Kim MH; Lin C-C, Assessing Monocyte Phenotype in Poly (γ-glutamic acid) Hydrogels Formed by Orthogonal Thiol-Norbornene Chemistry. Biomed. Mater 2021, 16(4), 045027.
49. Nguyen AK; Goering PL; Reipa V; Narayan RJ, Toxicity and Photosensitizing Assessment of Gelatin Methacryloyl-based Hydrogels Photoinitiated with Lithium Phenyl-2, 4, 6-Trimethylbenzoylphosphinate in Human Primary Renal Proximal Tubule Epithelial Cells. Biointerphases 2019, 14 (2), 021007. [PubMed: 31053032]
50. Kinstlinger IS; Calderon GA; Royse MK; Means AK; Grigoryan B; Miller JS, Perfusion and Endothelialization of Engineered Tissues with Patterned Vascular Networks. Nat. Protoc 2021, 16 (6), 3089–3113. [PubMed: 34031610]
51. Grim JC; Marozas IA; Anseth KS, Thiol-Ene and Photo-Cleavage Chemistry for Controlled Presentation of Biomolecules in Hydrogels. J. Control Release 2015, 219, 95–106. [PubMed: 26315818]
52. Gupta N; Lin BF; Campos LM; Dimitriou MD; Hikita ST; Treat ND; Tirrell MV; Clegg DO; Kramer EJ; Hawker CJ, A Versatile Approach to High-Throughput Microarrays Using Thiol-Ene Chemistry. Nat. Chem 2010, 2 (2), 138–145. [PubMed: 21124405]

53. Fujita M; Sasada M; Iyoda T; Fukai F, Involvement of Integrin-Activating Peptides Derived From Tenascin-C in Cancer Aggression and New Anticancer Strategy Using the Fibronectin-Derived Integrin-Inactivating Peptide. Molecules 2020, 25 (14), 3239. [PubMed: 32708610]
54. Alge DL; Azagarsamy MA; Donohue DF; Anseth KS, Synthetically Tractable Click Hydrogels for Three-Dimensional Cell Culture Formed Using Tetrazine–Norbornene Chemistry. Biomacromolecules 2013, 14 (4), 949–953. [PubMed: 23448682]
55. Wang M; Li W; Hao J; Gonzales A; Zhao Z; Flores RS; Kuang X; Mu X; Ching T; Tang G, Molecularly Cleavable Bioinks Facilitate High-Performance Digital Light Processing-based Bioprinting of Functional Volumetric Soft Tissues. Nat. Commun 2022, 13 (1), 1–18. [PubMed: 34983933]
56. Arkenberg MR; Lin C-C, Orthogonal Enzymatic Reactions for Rapid Crosslinking and Dynamic Tuning of PEG–Peptide Hydrogels. Biomater. Sci 2017, 5 (11), 2231–2240. [PubMed: 28991963]
57. Arkenberg MR; Koehler K; Lin C-C, Heparinized Gelatin-Based Hydrogels for Differentiation of Induced Pluripotent Stem Cells. Biomacromolecules 2022, 23 (10), 4141–4152. [PubMed: 36074748]
58. Jiang Z; Lin F-Y; Jiang K; Nguyen H; Chang C-Y; Lin C-C, Dissolvable Microgel-Templated Macroporous Hydrogels for Controlled Cell Assembly. Mater. Sci. Eng. C 2022, 112712.
59. McMurtrey RJ, Analytic Models of Oxygen and Nutrient Diffusion, Metabolism Dynamics, and Architecture Optimization in Three-Dimensional Tissue Constructs with Applications and Insights in Cerebral Organoids. Tissue Eng. Part C Methods 2016, 22 (3), 221–249. [PubMed: 26650970]
60. Cao X; Maharjan S; Ashfaq R; Shin J; Zhang YS, Bioprinting of Small-Diameter Blood Vessels. Engineering 2021, 7 (6), 832–844.
61. Corada M; Mariotti M; Thurston G; Smith K; Kunkel R; Brockhaus M; Lampugnani MG; Martin-Padura I; Stoppacciaro A; Ruco L, Vascular Endothelial–Cadherin is an Important Determinant of Microvascular Integrity In Vivo. Proc. Natl. Acad. Sci. U.S.A 1999, 96 (17), 9815–9820. [PubMed: 10449777]
62. Zheng Y; Chen J; Craven M; Choi NW; Totorica S; Diaz-Santana A; Kermani P; Hempstead B; Fischbach-Teschl C; López JA, In Vitro Microvessels for the Study of Angiogenesis and Thrombosis. Proc. Natl. Acad. Sci. U.S.A 2012, 109 (24), 9342–9347. [PubMed: 22645376]
63. Nguyen D-HT; Lee E; Alimperti S; Norgard RJ; Wong A; Lee JJ-K; Eyckmans J; Stanger BZ; Chen CS, A Biomimetic Pancreatic Cancer On-Chip Reveals Endothelial Ablation via ALK7 Signaling. Sci. Adv 2019, 5 (8), eaav6789.
64. Kinstlinger IS; Saxton SH; Calderon GA; Ruiz KV; Yalacki DR; Deme PR; Rosenkrantz JE; Louis-Rosenberg JD; Johansson F; Janson KD, Generation of Model Tissues with Dendritic Vascular Networks via Sacrificial Laser-Sintered Carbohydrate Templates. Nat. Biomed. Eng 2020, 4 (9), 916–932. [PubMed: 32601395]
65. Bernard AB; Lin C-C; Anseth KS, A Microwell Cell Culture Platform for the Aggregation of Pancreatic β-cells. Tissue Eng. Part C Methods 2012, 18 (8), 583–592. [PubMed: 22320435]
66. Giger S; Hofer M; Miljkovic-Licina M; Hoehnel S; Brandenberg N; Guiet R; Ehrbar M; Kleiner E; Gegenschatz-Schmid K; Matthes T, Microarrayed Human Bone Marrow Organoids for Modeling Blood Stem Cell Dynamics. APL Bioeng. 2022, 6 (3), 036101. [PubMed: 35818479]

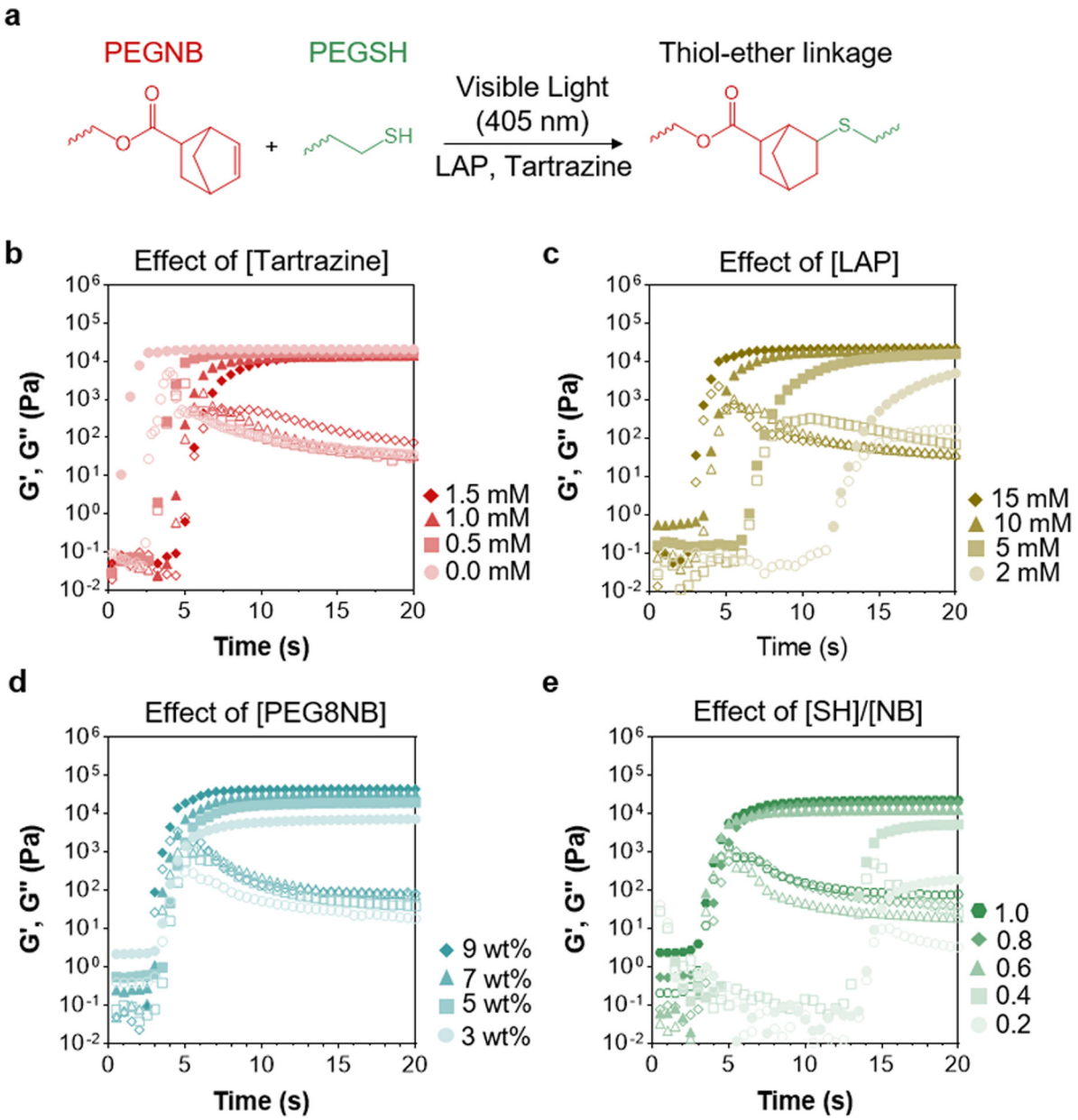

Figure 1. Optimization of thiol-norbornene crosslinking for DLP 3D printing.

(a) Schematic of thiol-norbornene photopolymerization. (b-e) *In situ* gelation behavior (storage modulus G'-solid symbols, and loss modulus G"-open symbols) of PEG8NB as a function of (b) photoabsorber tartrazine, (c) photoinitiator LAP, (d) macromer PEG8NB, and (e) reactive group ratio (R = [SH]/[NB]) under visible light (other parameters were fixed under the following conditions: 5 wt% PEG8NB, R=0.8 with PEG4SH, 10 mM LAP, 1.5 mM tartrazine).

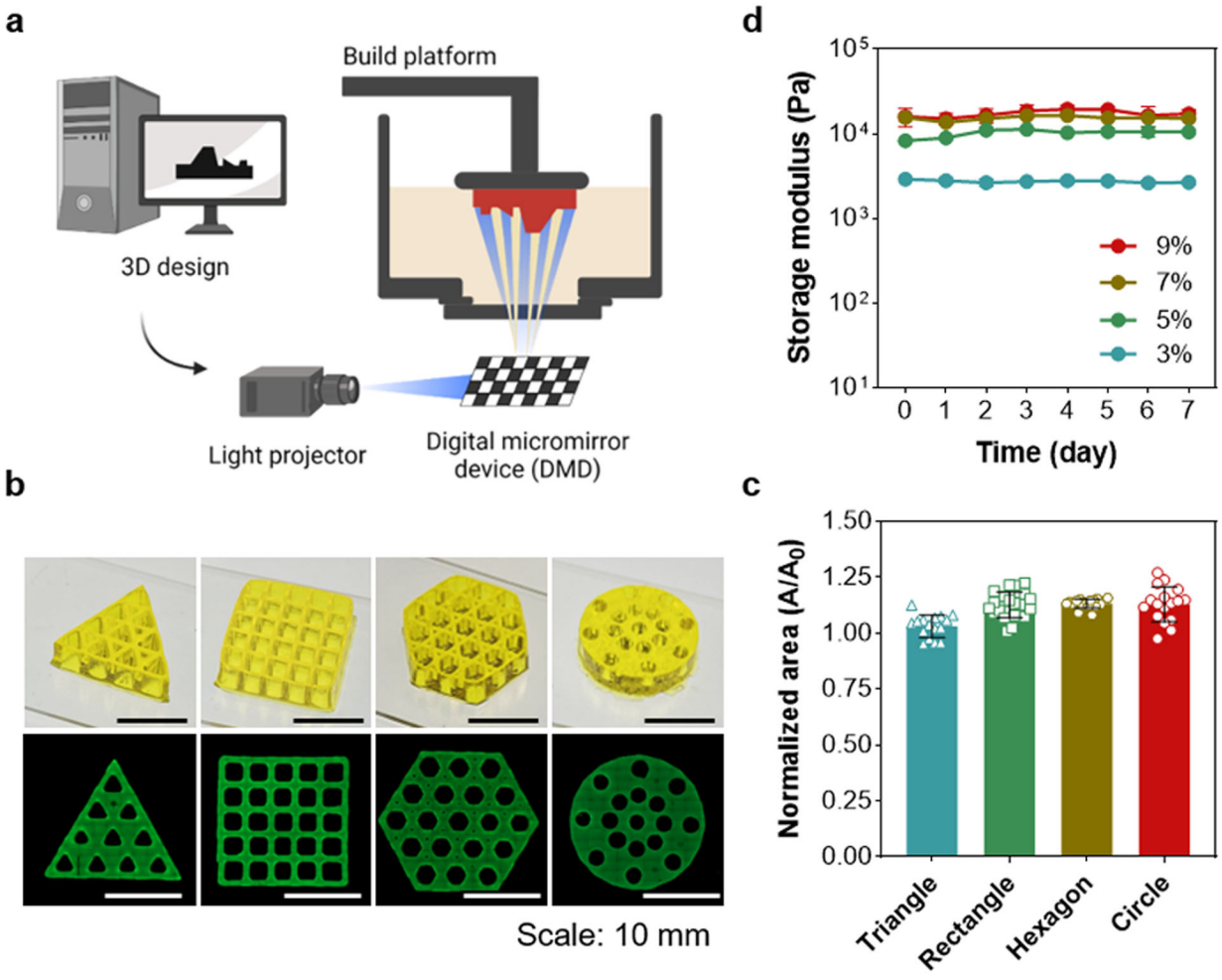

Figure 2. DLP 3D printing using PEG8NB/PEG4SH as the resin.

(a) Schematic of DLP 3D printing (created with BioRender.com). (b) Digital and fluorescence images of DLP printed complex PEGNB hydrogel structures (5% PEGNB, R=0.8 with PEG4SH, 10 mM LAP, 1.5mM tartrazine). (c) Printing fidelity of PEGNB hydrogel. (d) Effect of PEGNB concentration on stiffness of hydrogel.

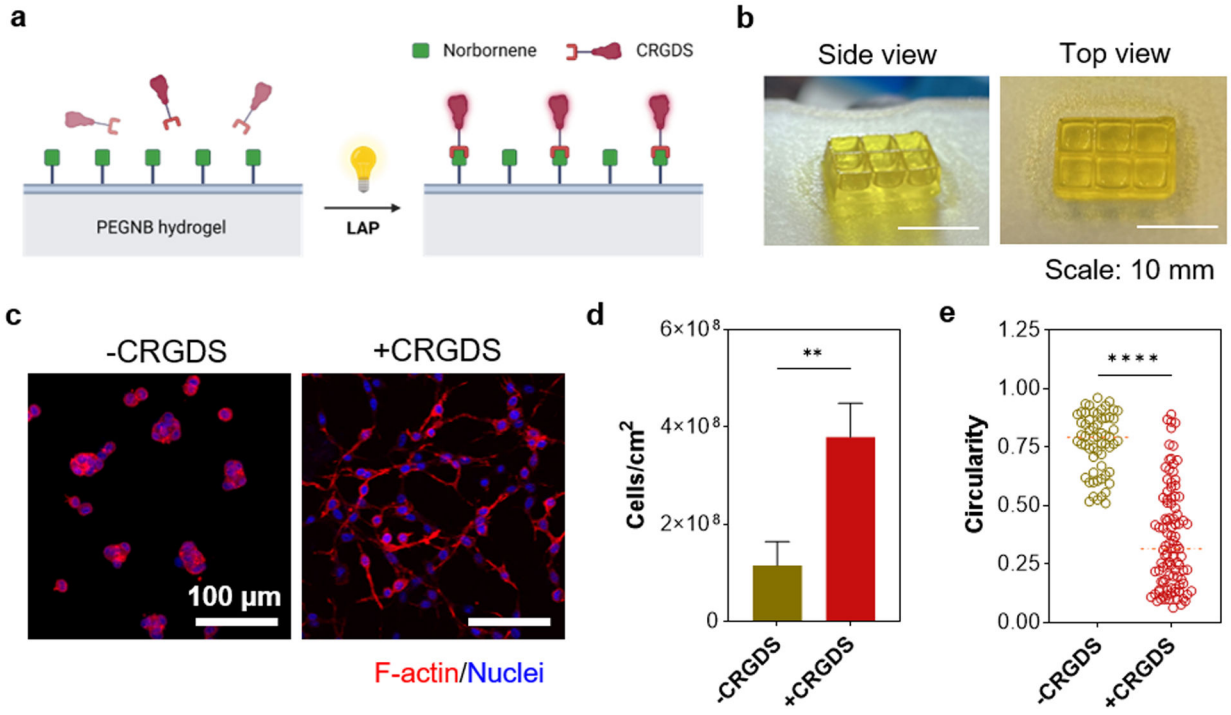

Figure 3. Surface modification via secondary thiol-norbornene photoclick reaction post DLP printing.

(a) Schematic of secondary surface immobilization of DLP 3D printed hydrogel using CRGDS (created with BioRender.com). (b) Digital images of DLP 3D printed PEGNB hydrogel for 2D cell culture model after DLP printing. (c) Effect of secondary surface immobilization on 3T3 fibroblast spreading. Quantification of the (d) number of cells per unit area, and (e) cell circularity (n=3; **p<0.01, ***p< 0.001; ****p< 0.0001, unpaired t-test).

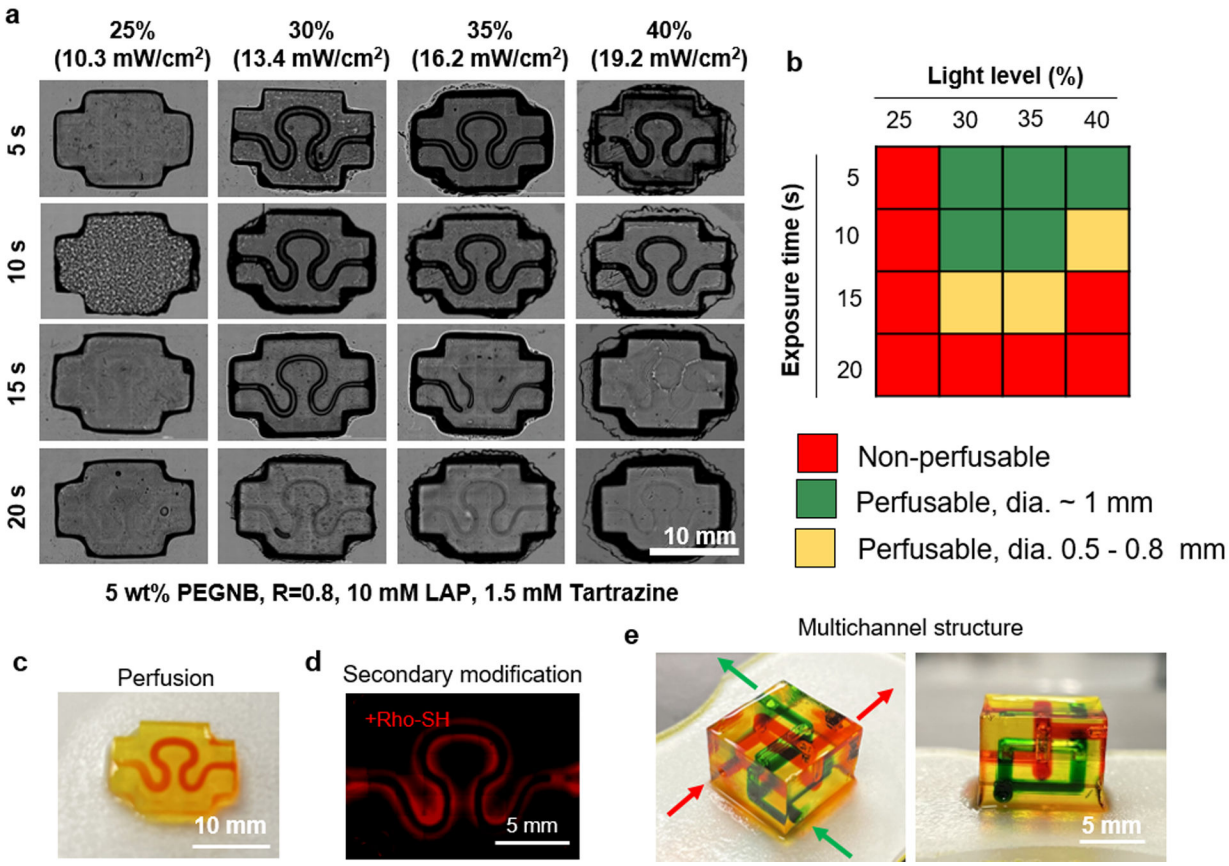

Figure 4. DLP printing of perfusable channels.

(a) Effect of exposure time and light intensity on the inner channel diameter of serpentine structure. (b) Qualitative evaluation of PEGNB hydrogel printability at different light intensity and exposure time using serpentine model. (c) Digital image of DLP 3D printed serpentine perfusable channel structures. (d) Effect of secondary immobilization on the inner-surface of microvasculature using Rho-SH. (E) Digital image of DLP 3D printed multi-channel microvasculature structures.

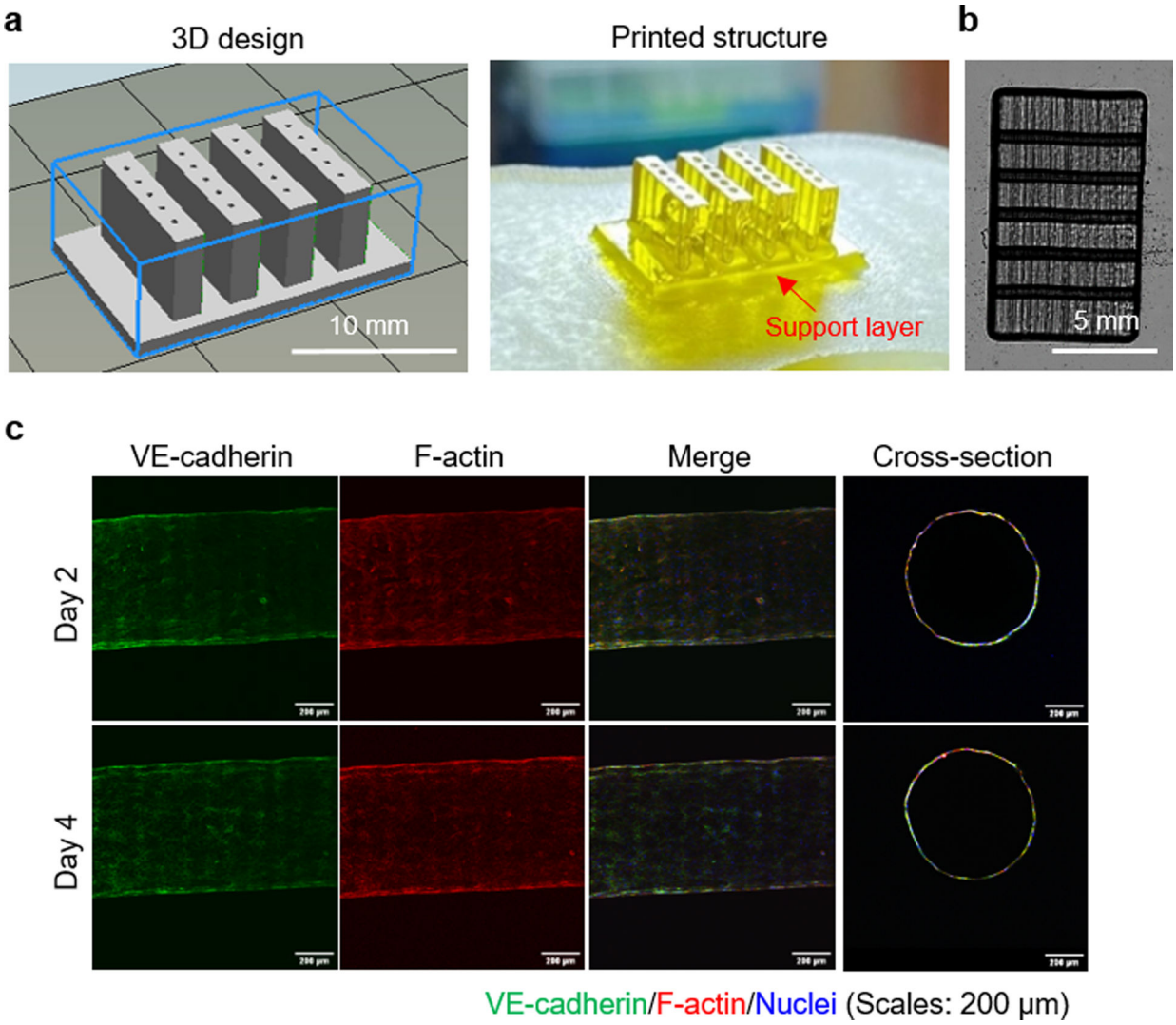

Figure 5. Endothelialization of DLP printed perfusable channels.

(a) 3D design and digital image of DLP printed microvasculature structure with a support layer. (b) Image of a detached slab of PEG8NB hydrogels with perfusable channels. (c) Immunostaining of an endothelized channel.

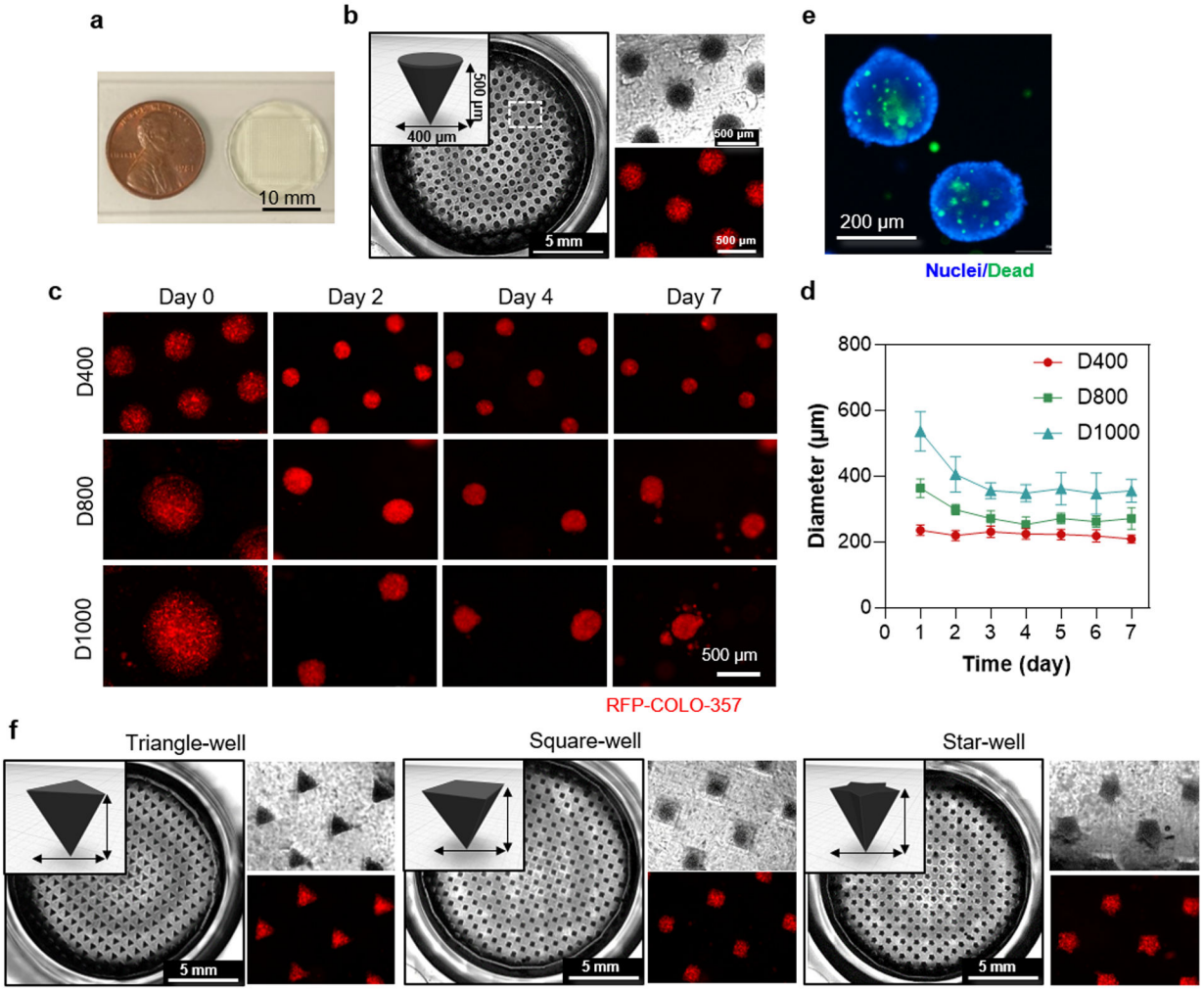

Figure 6. DLP printing of PEG-based microwells.

(a) Digital and microscopic images of DLP 3D printed PEGNB hydrogel for microwell. (b) Morphologies of RFP COLO-357 after seeding in cone-shaped PEGNB microwell. (c) Fluorescence images of COLO-357 spheroids with different microwell diameter, and (d) size differences over the time. (e) cell viability image after spheroid formation using ReadyProbes™ Cell Viability Imaging Kit. (f) Morphologies of RFP COLO-357 after seeding in different shape of microwell (triangle, square, and star respectively).